



# The Effect of Naturally Occurring Chronic Kidney Disease on the Micro-Structural and Mechanical Properties of Bone

Anna Shipov<sup>1\*</sup>, Gilad Segev<sup>1</sup>, Hagar Meltzer<sup>1</sup>, Moran Milrad<sup>1</sup>, Ori Brenner<sup>2</sup>, Ayelet Atkins<sup>1</sup>, Ron Shahar<sup>1</sup>

**1** Koret School of Veterinary Medicine, Hebrew University of Jerusalem, Rehovot, Israel, **2** Department of Veterinary Resources, Weizmann Institute, Rehovot, Israel

## Abstract

Chronic kidney disease (CKD) is a growing public health concern worldwide, and is associated with marked increase of bone fragility. Previous studies assessing the effect of CKD on bone quality were based on biopsies from human patients or on laboratory animal models. Such studies provide information of limited relevance due to the small size of the samples (biopsies) or the non-physiologic CKD syndrome studied (rodent models with artificially induced CKD). Furthermore, the type, architecture, structure and biology of the bone of rodents are remarkably different from human bones; therefore similar clinicopathologic circumstances may affect their bones differently. We describe the effects of naturally occurring CKD with features resembling human CKD on the skeleton of cats, whose bone biology, structure and composition are remarkably similar to those of humans. We show that CKD causes significant increase of resorption cavity density compared with healthy controls, as well as significantly lower cortical mineral density, cortical cross-sectional area and cortical cross-sectional thickness. Young's modulus, yield stress, and ultimate stress of the cortical bone material were all significantly decreased in the skeleton of CKD cats. Cancellous bone was also affected, having significantly lower trabecular thickness and bone volume over total volume in CKD cats compared with controls. This study shows that naturally occurring CKD has deleterious effects on bone quality and strength. Since many similarities exist between human and feline CKD patients, including the clinicopathologic features of the syndrome and bone microarchitecture and biology, these results contribute to better understanding of bone abnormalities associated with CKD.

**Citation:** Shipov A, Segev G, Meltzer H, Milrad M, Brenner O, et al. (2014) The Effect of Naturally Occurring Chronic Kidney Disease on the Micro-Structural and Mechanical Properties of Bone. PLoS ONE 9(10): e110057. doi:10.1371/journal.pone.0110057

**Editor:** Luc Malaval, Université Jean Monnet, France

**Received:** June 12, 2014; **Accepted:** September 9, 2014; **Published:** October 15, 2014

**Copyright:** © 2014 Shipov et al. This is an open-access article distributed under the terms of the Creative Commons Attribution License, which permits unrestricted use, distribution, and reproduction in any medium, provided the original author and source are credited.

**Data Availability:** The authors confirm that all data underlying the findings are fully available without restriction. All relevant data are within the paper.

**Funding:** This work was supported by the Israel Science Foundation (Grant No 151/08) to RS. The funders had no role in study design, data collection and analysis, decision to publish, or preparation of the manuscript.

**Competing Interests:** The authors have declared that no competing interests exist.

\* Email: anna.shipov@mail.huji.ac.il

† These authors contributed equally to this work.

## Introduction

Chronic kidney disease (CKD) is a growing public health concern worldwide, with increasing incidence in all age groups. The prevalence of moderate to severe CKD in the general population is reported to be as high as 8.5% [1,2]. The disease is irreversible and progressive in nature, and as it progresses, metabolic derangements worsen. This is particularly true in the ageing population, where CKD has become a major cause of morbidity and mortality.

CKD-associated bone diseases include several different types of bone pathologies, such as adynamic bone disease and osteomalacia which are characterized by low bone turnover, osteitis fibrosa cystica which is characterized by high bone turnover (due to secondary hyperparathyroidism) and mixed uremic osteodystrophy which is characterized by either high or low turnover and abnormal mineralization [3].

One of the inevitable metabolic consequences of CKD is secondary renal hyperparathyroidism (SRH) [4]. The pathophysiology of SRH is complex and involves phosphorus retention

leading to hyperphosphatemia, ionized hypocalcemia, decreased circulating 1,25-dihydroxyvitamin D (calcitriol) concentration and increased concentrations of parathyroid hormone (PTH) and fibroblast growth factor 23 [FGF23, [5]]. FGF23, which has been shown to have a pivotal role in mineral homeostasis, is produced mainly by osteocytes and osteoblasts [6]. Serum levels of FGF23 increase already in the early stages of CKD, when patients are still normo-phosphatemic and have normal PTH levels [7–9]. When PTH levels increase, they promote bone resorption, and persistently high PTH concentrations, as documented in CKD patients, eventually lead to, osteopenia, and increased risk of pathological fractures [10].

It is widely recognized that bone fragility increases markedly in patients with CKD, and that fracture risk increases with progression of the disease [11–13]. The risk of pathological fractures has been reported to increase by 9% with each 200-pg/mL increase in PTH concentration, and by 72% with PTH concentrations above 900 pg/mL (reference range, 150–300 pg/mL), [10]. Furthermore, the United States Renal Data System

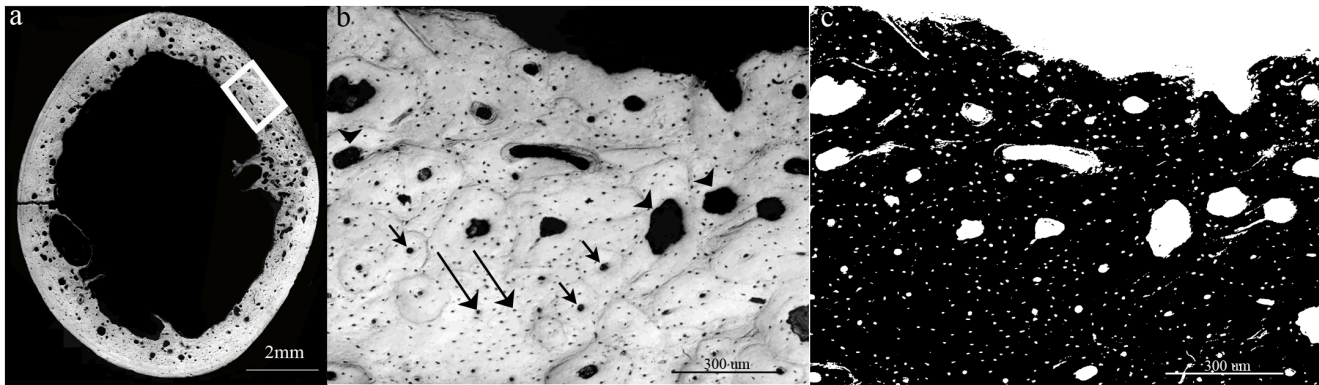


**Figure 1. Bone cavity analysis.** (a) Light microscopy image of a typical transverse cross section of the bone created by stitching together of many individual images. Classification of voids was performed on based on their size. (b) An individual image from the cross sectional image (marked by a white rectangle in image a). (c) Each image was first binarized, separating it into 'bone' (white) and 'void' (black) (right image). Cavities within the range of 9–50  $\mu\text{m}^2$  were considered to be lacunae (long arrows), cavities within the range of 151–2000  $\mu\text{m}^2$  were considered to be Haversian canal (short arrows) and cavities larger than 2000  $\mu\text{m}^2$  were considered resorptive lesions (arrowheads). doi:10.1371/journal.pone.0110057.g001

identified a 4-fold greater risk of hip fractures in human dialysis patients as compared to the general population [11].

The precise structural and compositional changes in the skeleton that occur in CKD patients, are not entirely clear. Data regarding the nature of these changes is crucial to the understanding of the skeletal consequences of CKD, since they determine the quality of bone material and the quantitative deterioration of material's mechanical properties. Most previous studies were based on data collected from human patients or from rodent models. For obvious reasons, studies conducted on human patients are subjected to severe inherent limitations, primarily the need to rely on non-invasive or minimally invasive (biopsy) methods. Biopsies, while a valuable diagnostic tool, by their nature provide data relevant to a very small region in a bone, and therefore can provide only limited information. Noninvasive methods used in human patient studies, such as determination of bone mass (or apparent mineral density) by dual x-ray absorptiometry (DEXA) provide imprecise information because of technical limitations, as described eloquently by Parfitt [14]. The main limitations of DEXA include its reliance on a 2-D proxy of mineral density ( $\text{g}/\text{cm}^2$ ) measurement rather than true 3-D density, and the inability to obtain separate data for cortical and trabecular bone. Peripheral quantitative computed tomography (pQCT) provides true 3-D information and is therefore a valuable tool, however its resolution is in the mm range.

On the other hand, use of model animals (almost exclusively mice and rats), while allowing the use of a wide array of testing methods, is hindered by the fact that in most studies, CKD is induced by non-physiologic means, mostly partial nephrectomy [15]. This obviously does not mimic with precision the disease in human patients, and may affect the skeleton in ways which are subtly (or even substantially) different from those caused by the natural course of the disease in humans. Moreover, the structure and architecture of rat and mouse cortical bone differs greatly from that of human cortical bone, as shown recently by Shipov *et al* and Bach-Gansmo *et al* [16,17]. Therefore, the ability to directly extend the observed effects of artificially-induced CKD in the rat skeleton to the effects of naturally-occurring CKD in the human skeleton is limited.

The course, pathology and pathophysiology, diagnosis and treatment of feline CKD mirror those of the human disease very closely, and the disease is very prevalent in the feline population

[18]. Another major advantage of studying the effects of CKD in cats is that the bones of mature cats are structurally and compositionally very similar to those of humans, both consisting mostly of remodeled secondary osteons [19].

Here we present a detailed study of the skeletal changes, both structural and mechanical, in cats with naturally occurring CKD. In this study we compare the femora and vertebra of cats diagnosed with CKD and those of age-matched cats with normally functioning kidneys.

## Materials and Methods

### 2.1 Animals and data collection

The study was prospective, based on the patient population of the Veterinary Teaching Hospital of the Hebrew University of Jerusalem, and was approved by the institutional animal care and use committee. Cats considered for the study either died or were euthanized at their owners' request after medical management had failed. Euthanasia was performed using 200 mg/kg pentobarbital (CTS chemical industries LTD, Israel) administered intravenously. Cats were enrolled only after their owners had signed an informed consent form and donated the body to science. The study group consisted of 13 cats diagnosed with Stage III or IV CKD, based on the classification scheme of the International Renal Interest Society guidelines [20], for at least 6 months prior to death or euthanasia. These criteria included documentation of persistent azotemia (3 occasions, at least 2 weeks interval, serum creatinine concentration  $>2.8$  mg/dL), urine specific gravity  $<1.020$  and ultrasonographic changes consistent with CKD. CKD was additionally confirmed in all cats by histopathological examination showing moderate to severe interstitial nephritis accompanied by moderate to severe fibrosis.

The control group included 13 healthy cats without any clinicopathologic signs of CKD (e.g., normal creatinine, concentrated urine) that died or were euthanized in the Veterinary Medical Teaching Hospital due to reasons unrelated to diseases of the urinary system. Cats with concurrent metabolic diseases that could potentially affect the skeleton were excluded, as were cats that were treated for more than 2 weeks during the 6 months prior to their death with medications that could alter bone metabolism (e.g., vitamin D derivatives, corticosteroids).

**Table 1.** Morphometric characteristics of cortical bone of the distal femur in CKD and healthy controls by light microscopy.

| Light microscopy morphometry | CKD (mean ±SD) | Controls (mean ±SD) | P value     |
|------------------------------|----------------|---------------------|-------------|
| <i>Osteocytic lacunae</i>    |                |                     |             |
| Size [ $\mu\text{m}^2$ ]     | 33.9±3.1       | 33.1±3.9            | 0.60        |
| Density [ $\text{mm}^{-2}$ ] | 510±55         | 524±106             | 0.70        |
| <i>Haversian canals</i>      |                |                     |             |
| Size [ $\mu\text{m}^2$ ]     | 481±115        | 411±48              | 0.10        |
| Density [ $\text{mm}^{-2}$ ] | 22.3±4.3       | 23.3±4.6            | 0.58        |
| <i>Resorption cavities</i>   |                |                     |             |
| Size [ $\mu\text{m}^2$ ]     | 10,342±11,888  | 12,406±25,258       | 0.78        |
| Density [ $\text{mm}^{-2}$ ] | 2.2±2.4        | 0.4±0.1             | <b>0.04</b> |

doi:10.1371/journal.pone.0110057.t001

## 2.2 Sample collection and preparation

Blood and serum samples from all cats were collected *antemortem* for complete blood count and biochemical analysis. Sera were stored at  $-80^\circ\text{C}$  for determination of PTH and vitamin D levels.

Tissue sample collection was performed within 12 hours of death. The right femora and lumbar vertebrae were carefully removed and cleaned of all soft tissue, wrapped in saline-soaked gauze, placed in a sealed plastic bag and stored at  $-20^\circ\text{C}$  until testing. Kidney samples were harvested and stored in 10% formalin for histologic evaluation.

## 2.3 Light microscopy

Thin transverse slices (400 microns thick) of the mid-diaphyseal region of all right femora were cut by a water-cooled slow-speed diamond saw (Buehler Isomet low Speed saw, USA). The slices were then polished by increasingly fine grit (Buehler Minimet Polisher, USA), from 320 grit to 1  $\mu\text{m}$  diamond paste. Transverse cross-sections of all cortical samples were viewed by reflective light microscopy (Olympus BX-51) and their detailed architecture characterized by analysis of images captured by a dedicated high-resolution camera (Olympus DP 71, 12 MegaPixels).

Quantitative analysis of the transverse cross-sectional images, particularly quantification of voids and their classification, was performed with a public domain image processing software (ImageJ, NIH, v. 1.44p). Several microstructural parameters were measured, such as the number, size and density of the osteocytic lacunae, Haversian canals and resorption cavities within each cross section [21]. Specifically, each cross-sectional image was first binarized by selection of an appropriate threshold, separating it into 'bone' (white) and 'void' (black) entities [22], (Fig. 1 a, b). Next, the ImageJ 'analyze particles' command was applied to each cross-section to identify all individual voids within it. This command analyzes each void by its size and reports the results in a tabular form (see Figure 1) [23]. Based on sizes of osteocytic

lacuna and Haversian canals reported in the literature [24–27] voids with an area in the range of 9–150  $\mu\text{m}^2$  were considered to be osteocytic lacunae, voids with an area in the range of 151–2000  $\mu\text{m}^2$  were considered to be Haversian canals, while voids larger than 2000  $\mu\text{m}^2$  were considered resorption cavities which are in the process of remodeling [21]. Voids smaller than 9  $\mu\text{m}^2$  were considered to be artifacts. Images were also visually examined by two of the authors (AS and HM) and the results of thresholding and void categorization were manually corrected if indicated. Overall porosity was calculated as the ratio of total void area (i.e. resorption cavities, lacunae and blood vessels) to total bone area.

## 2.4 Mechanical testing

Mechanical properties of cortical bone were evaluated using four-point bending tests performed on bone beams prepared from the cranial aspect of the mid-diaphyseal cortical region of the right femora. Beam sizes were 20 mm×1.5 mm×1 mm (long dimension along the bone axis).

Mechanical testing was performed with the samples immersed in saline, using a custom-built micromechanical-testing device as previously described [28]. All samples were thawed immediately before testing for one hour at room temperature. The beams were placed within a saline-containing testing chamber that had a stationary anvil attached to its wall [28]. This anvil consisted of two supports which were 15 mm apart. A movable double-pronged loading anvil was attached to a load-cell (model 31, Honeywell Sensotec, Columbus, OH, USA), which was in turn attached to a high-precision linear motor (PI GmbH, Karlsruhe, Germany). The loading anvil had a span of 5 mm between its two prongs, which were centered between the two supports of the stationary anvil.

The upper prongs were brought into contact with the tested beams at a predetermined preload (2N), the chamber was filled with physiologic saline solution at room temperature until the

**Table 2.** Morphometry of cortical bone of the mid-diaphyseal femur in CKD and healthy controls.

| Microtomography                                 | CKD (mean ±SD) | Controls (mean ±SD) | P value     |
|---|----------------|---------------------|-------------|
| Cortical cross sectional area ( $\text{mm}^2$ ) | 28.5±3.6       | 32.2±5.5            | <b>0.04</b> |
| Cross-sectional thickness (mm)                  | 1.1±0.2        | 1.2±0.2             | <b>0.03</b> |
| Mean polar area of inertia ( $\mu\text{m}^4$ )  | 432±95         | 520 ±154            | 0.08        |

doi:10.1371/journal.pone.0110057.t002

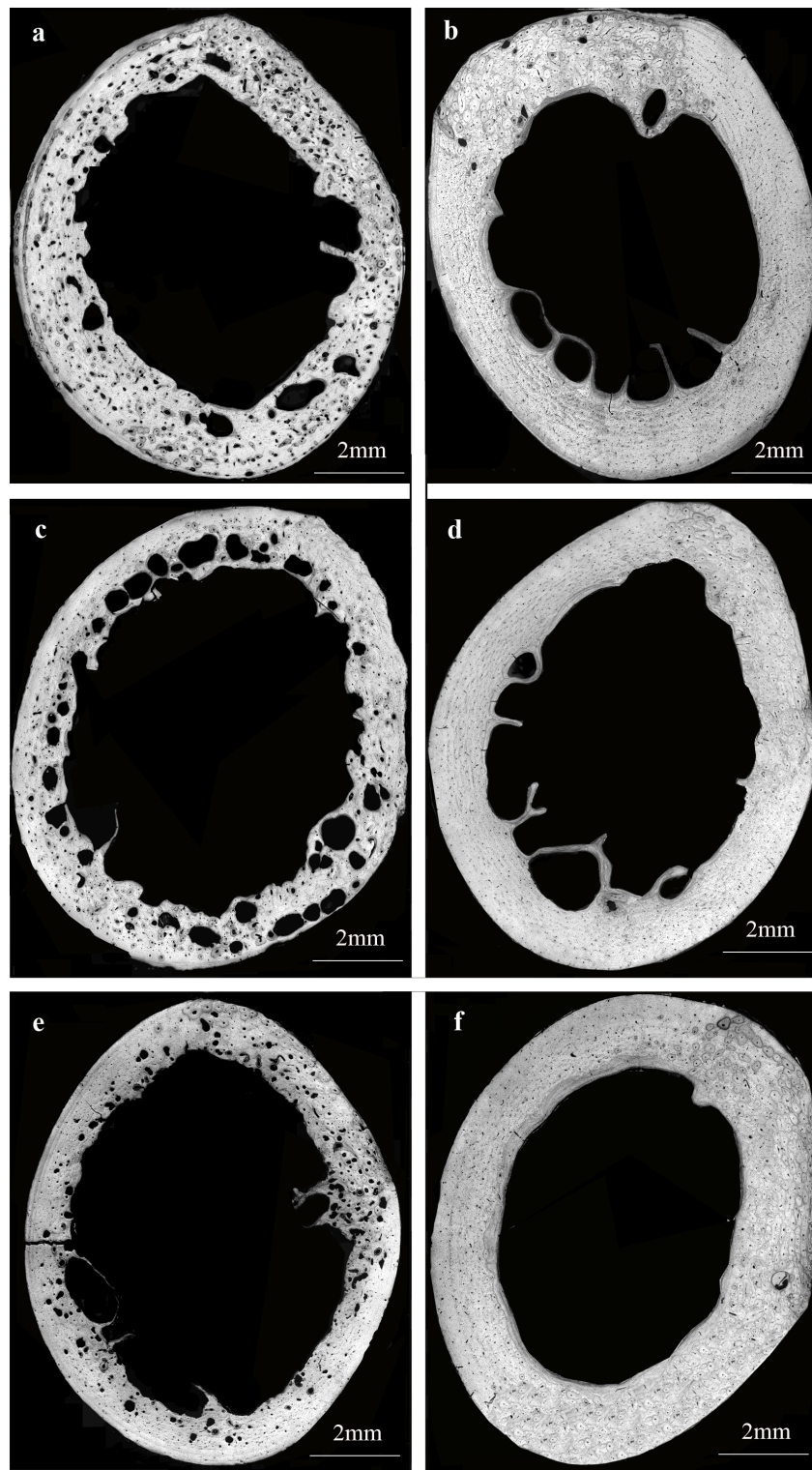


**Figure 2. Light microscopy images of three transverse cross-sections of the femoral mid-diaphysis of (a, c, e) cats with CKD and (b, d, f) healthy cats.** Note dramatic increase in unfilled resorption cavities in CKD cats compared to the healthy cats.  
doi:10.1371/journal.pone.0110057.g002

samples were fully immersed, and bending tests were conducted under displacement control at a rate of  $500\ \mu\text{m}/180\ \text{seconds}$  up to failure. Force-displacement data were collected by custom-written software (LabView, National Instruments, Texas, USA) at 50 Hz.

Load and displacement values were converted to stress and strain, respectively, based on beam theory [29]. The stress-strain curves were used to estimate Young's modulus of the beam material, as well as yield and failure stresses and strains. It should be noted that

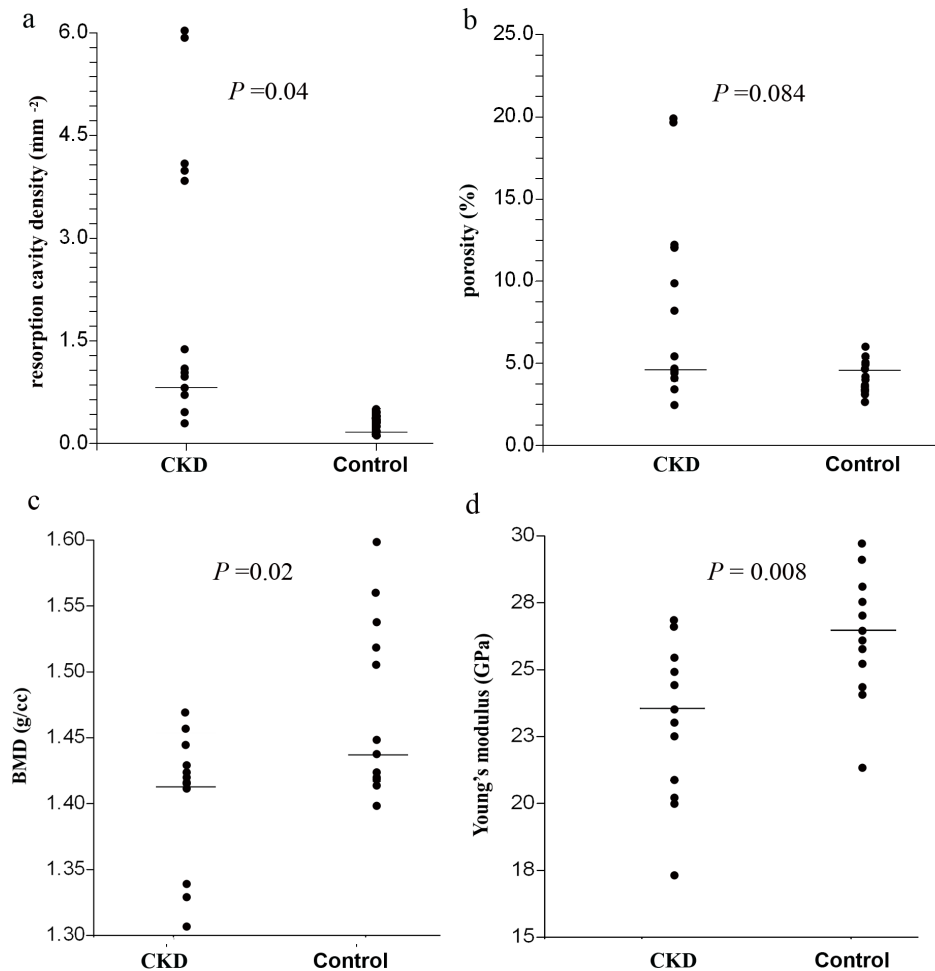


**Figure 3. Dot plots depicting the data of CKD and control cats; the horizontal line represents the median.** (a) resorption cavity density (b) porosity, (c) BMD and (d) Young's modulus.  
doi:10.1371/journal.pone.01110057.g003

care was taken to minimize shear deformation at the supports by maintaining a ratio of distance between supports/beam depth of 15:1 [30,31]. Yield point was determined for each beam as the point at which a line parallel with the linear portion of the stress-strain curve and offset by 0.03% strain intersected with this curve [32].

### 2.5 Microstructural characterization by Micro-CT

All cortical beams, the right femur and the 6<sup>th</sup> and 7<sup>th</sup> lumbar vertebrae were scanned by microCT (Skyscan 1174 compact micro-CT scanner, Belgium), with the beams scanned prior to mechanical testing. Analyses were performed on the entire beam, the mid-diaphyseal femoral cortex (cortical bone analysis), and in the distal femoral metaphyses and vertebral bodies (cancellous bone analysis).

The X-ray source was set at 50 kVp and 800  $\mu$ A. A total of 450 projections were acquired over an angular range of 180°. The samples were scanned with an isotropic voxel size of 11.1  $\mu$ m for the cortical bone beams and 19.6  $\mu$ m for the femoral cortex and cancellous bone of both the femora and vertebrae. Integration time for all scans was 4500 ms, and a 0.25 mm aluminum filter was used. Scans were reconstructed and analyzed using commercial software (NRecon Skyscan software, version 1.6.1.2 and CT

analyser Skyscan software, version 1.9.3.2, respectively). Cortical bone mineral density (BMD) of the beams was determined based on calibration with 2 phantoms of known mineral density (0.25 g/cm<sup>3</sup> and 0.75 g/cm<sup>3</sup>) supplied by SkyScan, which were scanned under exactly the same condition as were the bone specimens.

### 2.6 Statistical analysis

The distribution of continuous parameters (normal vs. non-normal) was assessed using the Shapiro-Wilk's test. Normally and non-normally distributed continuous parameters were compared between the study and the control group using Student's t-test and Mann-Whitney U test, respectively. Gender proportion between the study group and the control groups was compared using the Fischer Exact test. Correlations between continuous parameters (e.g., biomechanical parameters and PTH concentration) were performed using the Pearson or the Spearman Rank correlation test, according to data distribution. For all tests  $P<0.05$  was considered statistically significant. All calculations were performed using a statistical software (SPSS 17.0 for Windows, SPSS Inc; Chicago, IL, USA).

## Results

### 3.1 Animals

The study population included 26 cats, of which 13 were diagnosed with CKD and 13 were healthy controls. There were eight males and five females in the study group and six males and seven females in the control group, with no gender proportion differences between the study groups. Mean body weight was significantly lower in cats with CKD compared with healthy controls ( $2.8 \pm 0.6$  kg vs.  $3.7 \pm 0.9$  kg, respectively;  $P = 0.01$ ). There was no statistically significant difference in mean age between the study and control groups ( $10.5 \pm 5.6$  years compared to  $9.7 \pm 3.9$  years, respectively;  $P = 0.7$ ).

### 3.2 Clinical pathology

Median serum creatinine concentration within the CKD group was 8.2 mg/dL (range 3.5–16.0 mg/dL) compared with a median of 0.9 mg/dL (range 0.6–1.2 mg/dL) [reference interval (RI), 0.5–1.6 mg/dL] of the control group. Three cats in the study group (23%) were classified as Stage III CKD, and the rest (77%) were classified as Stage IV CKD. Median phosphorous concentration in the study group was 8.8 mg/dL (range 5.3–21.7 mg/dL; RI, 3.0–6.2 mg/dL). Median concentration of ionized calcium in the study group was 0.80 mmol/L (range 0.65–1.01 mmol/L; RI, 0.9–1.4 mmol/L). PTH concentration, available for five cats of the study group, had a median concentration of 15.70 pmol/L (range, 0.9–32.9 pmol/L; RI, 0.4–2.5 pmol/L). Vitamin D concentration was below normal in five out of the seven cats in which it was measured (median 63 nmol/L, range 35–143 nmol/L; RI 65–170 nmol/L).

### 3.3 Cortical bone architecture

The results of the architectural analysis are presented in Table 1 (microscopy) and Table 2 (microCT). CKD-affected cats had significantly higher density of resorption cavities compared to healthy controls (Table 1, Figures 2, 3a). Other structural parameters were not significantly different between the groups. Porosity tended to be higher in the CKD group, however the difference between groups did not reach statistical significance ( $P = 0.084$ , Figure 3b).

Micro-CT analysis of cortical bone of the femoral diaphysis showed significantly lower cortical cross-sectional area and cross-sectional thickness in CKD cats (Table 2). Mean polar area moment of inertia tended to be lower in the CKD group, but the differences did not reach statistical significance ( $P = 0.083$ ) (Table 2).

### 3.4 Cortical mineral density

Cortical mineral density of CKD cats was lower by 4.8% compared to controls, ( $P = 0.02$ , as shown in Figure 3c).

### 3.5 Mechanical properties of cortical bone

Table 3 and Figure 3 present a comparison of several mechanical properties of cortical bone material between the CKD and control groups. Bones from the CKD group were shown to have inferior mechanical properties compared to the control group, in particular lower stiffness (Young's modulus), lower yield stress, and lower ultimate stress (Table 3, Figure 3).

Correlation could not be demonstrated between PTH levels and any of the mechanical properties of the cortical bone.

### 3.6 Architecture of trabecular bone

Analysis of cancellous bone in the 6<sup>th</sup> and 7<sup>th</sup> lumbar vertebrae and in the distal femur revealed significantly lower trabecular thickness and bone volume over total volume (BV/TV) in bones belonging to the CKD group, compared with control cats (Figure 4).

## Discussion

This study demonstrates that advanced CKD in cats results in deterioration of bone quality, in particular a dramatic increase of resorption cavities and decreased bone mineral density. These results provide insight into skeletal changes occurring in human CKD due to the similarity between cats and humans in terms of the pathophysiology of the syndrome and the type of bone architecture.

To the best of our knowledge, this is the first study to measure the detailed mechanical and structural effects of CKD on the skeleton of an animal model with *naturally occurring* CKD. Feline and human CKD have very similar clinicopathologic features and progression, therefore cats are superior models compared to rodents in which pharmaceutical and surgical interventions are usually employed to induce kidney disease [33–36]. Furthermore, the cat skeleton shows great similarities to human bone, in particular because it remodels continuously throughout life and therefore consists mostly of secondary osteons. Rodent bones on the other hand are remarkably different from those of human bones in terms of type, architecture, structure and biology. Most dramatically, rodent cortical bone does not remodel [16,17]. Therefore similar clinicopathologic circumstances, such as those occurring due to CKD, may affect rodent bones differently from human (or cat) bones.

We found that naturally occurring CKD results in several alterations to the architecture and morphology of the bones of the skeleton. Cortical thickness was found to be decreased by approximately 17% in CKD cats compared with controls. This change compromises the mechanical performance of long bones, by reducing their flexural stiffness and is likely to lead to increased fracture risk. Previous studies conducted in human patients with CKD showed similar tendencies, however with much smaller changes. For instance, a recent study documented 4.2% increase

**Table 3.** Mechanical properties of the cortical bone of CKD and control groups.

| Parameter                     | CKD (mean $\pm$ SD)            | Controls (mean $\pm$ SD)       | P value     |
|-------------------------------|--------------------------------|--------------------------------|-------------|
| <b>Young's modulus (GPa)</b>  | <b>23.5<math>\pm</math>2.9</b> | <b>27.1<math>\pm</math>2.8</b> | <b>0.01</b> |
| <b>Yield stress (MPa)</b>     | <b>151<math>\pm</math>18</b>   | <b>166<math>\pm</math>14</b>   | <b>0.04</b> |
| Yield strain (millistrain)    | 5.6 $\pm$ 0.8                  | 5.6 $\pm$ 0.4                  | .95         |
| <b>Ultimate stress (MPa)</b>  | <b>185<math>\pm</math>16</b>   | <b>205<math>\pm</math>15</b>   | <b>0.01</b> |
| Ultimate strain (millistrain) | 8.6 $\pm$ 1.0                  | 8.1 $\pm$ 0.4                  | 0.37        |

doi:10.1371/journal.pone.0110057.t003

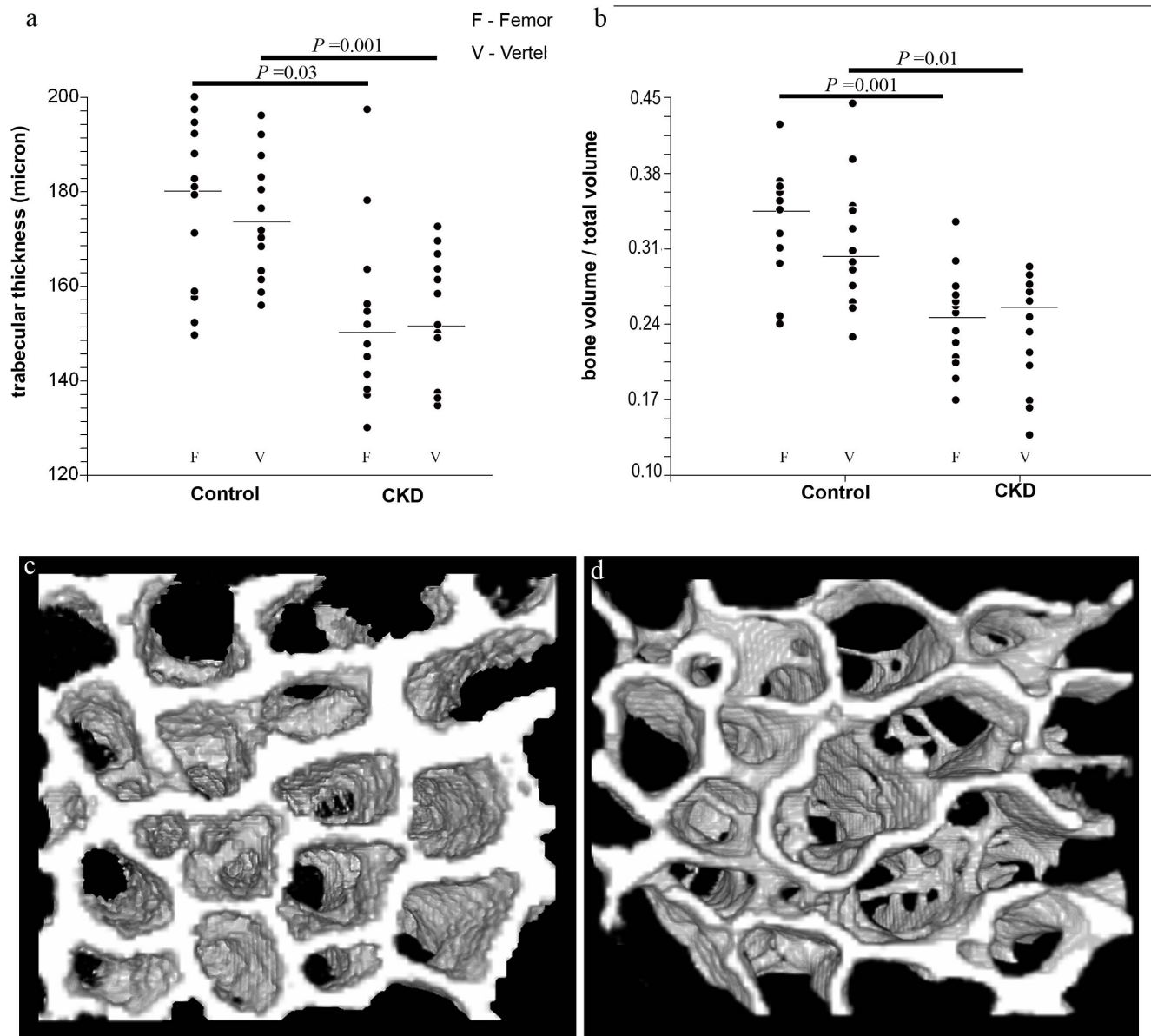


**Figure 4. Trabecular bone analysis: Trabecular thickness (a) and bone volume/total volume (BV/TV, b) in the cancellous bone of CKD and control cats for both the femora (F) and the vertebrae (V).** Data are presented as dot plots. The horizontal line represents the median. Data from the femur and vertebra are similar within the study groups; however, there is a significant difference for both parameters between the study and the control groups. Micro-CT scans of cancellous bone of a control (c) and CKD (d) cat. doi:10.1371/journal.pone.0110057.g004

in porosity, 2.9% decrease in cortical area and 2.8% decrease in cortical thickness, indicating progressive loss of cortical bone [37]. These results, like those of other human studies, were based on DEXA and high resolution peripheral quantitative CT. These methods have been shown to be limited in precision in terms of bone volume quantification due to inability to separate cortical from cancellous bone (DEXA), and low-resolution volumetric measurements, compared to microCT and whole bone sampling [38].

Overall cortical porosity in cats with advanced CKD tended to be somewhat higher compared with controls (Figure 3b), but this difference did not reach statistical significance, most likely due to small group size and biological variation. However, the density (number per unit area) of resorption cavities in CKD patients is

greatly increased (5-fold,  $2.22/\text{mm}^2$  vs.  $0.41/\text{mm}^2$ ,  $P=0.04$ ). Such a difference is expected to affect mechanical behavior of long bones radically, and is likely to play an important role in the increased fragility of CKD patients. Previous studies in a rat model demonstrated that persistently elevated PTH concentrations result in high bone turnover, exhibited as elevated numbers and size of osteoclasts, increased osteoblastic activity and enhanced bone resorption [33]. Consequently, these studies found extensive endocortical, intracortical and periosteal resorption, resulting in a dramatic increase in cortical porosity (9.75% compared to 0%). It should be noted however that these results were observed in rat bone, which normally does not remodel, as oppose to cat (and human) bone.

Bone mineral density is another major determinant of bone quality, and the current clinical standard for prediction of fracture risk in osteoporotic patients [39]. Therefore, determining the influence of CKD on BMD was a major objective of this study. The cortical mineral density of cats with CKD was significantly lower compared to controls. It should be noted that despite appearing small, this decrease (4.8%) is clinically significant, as even a small decrease in BMD substantially decreases the stiffness of the bone and increases fracture risk [40], since the relationship between them is exponential [41]. A decrease in BMD was also reported in various studies in humans CKD patients, with a wide range of values [1.3% to 17.5%; [37,42,43]]. However, these studies were based on areal BMD ( $\text{g}/\text{cm}^2$ , using DEXA), histomorphometry or pQCT, while the current study measured volumetric BMD at high resolution and precision using microCT [38,44].

Reliable measurement of material properties requires precise and accurate mechanical testing. Such testing is difficult to achieve in rodents due to the small size of their bones, which are often tested by bending tests of whole bones, using the 3-point bending technique. Results are dependent upon the geometry of the bones and mechanical properties of the material, often leading to underestimation of Young's modulus [45,46]. The size of cat bones allowed us to prepare cortical bone beams, enabling accurate and reliable assessment of the material properties using four-point bending testing. Furthermore, four-point bending tests of beams allowed us also to measure other material properties, like yield and strength, and to document significant decrease in yield stress and failure stress in the cortical bone of the CKD cats compared to controls.

This study demonstrates that the cortical bone material of CKD cats is less stiff and more prone to micro-damage which occurs at lower loads, and will result in increased bone fragility. In particular, Young's modulus of the cortical bone, which reflects the stiffness of the material, was shown here to be significantly lower in the CKD group (23.5 GPa vs 27.1 GPa, respectively,  $P = 0.008$ ). The lower Young's modulus in CKD cats compared with controls is most likely due to a combination of higher porosity and lower BMD.

Cancellous bone is also significantly affected by CKD, as reflected by decreased trabecular thickness and lower bone volume

(BV/TV). Furthermore, the effect on cancellous bone was multi-site, shown to occur both in the vertebral bodies as well as in the long bones. Both changes (trabecular thickness and BV/TV) negatively affect bone quality and were shown to be associated with increased risk for fracture [47].

Since this study was based on cats with naturally occurring kidney disease, some variability existed among them in terms of the severity and the chronicity of the disease. Furthermore, the number of cats included in this study was relatively small, though comparable to numbers typically seen in published rodent model studies. It should also be noted that cats with advanced CKD often exhibit decreased appetite and thus might fail to consume enough food to meet their caloric requirements. Such nutritional deficiencies, as in human patients, might contribute to their decreased bone quality. Additionally, all of the cats in this study had a single etiology (interstitial nephritis, which is the etiology in more than 70% of cases with CKD in cats [18]), whereas human patients with CKD have multiple etiologies (e.g., diabetic nephropathy, transplant patients, etc.). Nevertheless, slowly progressive natural disease represents the human syndrome and its consequences, including renal osteopathy, much better than artificially-induced rodent models.

In conclusion, the current study demonstrates the deleterious effects of CKD on remodeled (secondary osteonal) bone quality and strength, including increased bone resorption, decreased BMD, and inferior mechanical and structural properties. Due to these changes, the bones of CKD patients become more fragile. Since many similarities have been demonstrated between human and feline CKD patients, in terms of the clinic-pathologic features of the syndrome, as well as bone-associated effects, cats are an extremely suitable and relevant animal model for studying the development of bone abnormalities in humans suffering from CKD.

## Author Contributions

Conceived and designed the experiments: AS GS HM MM RS. Performed the experiments: AS GS HM MM AA OB RS. Analyzed the data: AS GS HM MM AA RS. Contributed reagents/materials/analysis tools: RS OB. Wrote the paper: AS HM GS MM OB AA RS.

## References

- Lora CM, Daviglius ML, Kusek JW, Porter A, Ricardo AC, et al. (2009) Chronic kidney disease in United States Hispanics: a growing public health problem. *Ethn Dis* 19: 466–472.
- McClellan WM, Plantinga LC (2013) A public health perspective on CKD and obesity. *Nephrol Dial Transplant* 28 Suppl 4: iv37–iv42.
- Spasovski GB, Bervoets AR, Behets GJ, Ivanovski N, Sikole A, et al. (2003) Spectrum of renal bone disease in end-stage renal failure patients not yet on dialysis. *Nephrol Dial Transplant* 18: 1159–1166.
- Levin A, Bakris GL, Molitch M, Smulders M, Tian J, et al. (2007) Prevalence of abnormal serum vitamin D, PTH, calcium, and phosphorus in patients with chronic kidney disease: results of the study to evaluate early kidney disease. *Kidney Int* 71: 31–38.
- Cozzolino M, Ciceri P, Volpi EM, Olivi L, Messa PG (2009) Pathophysiology of calcium and phosphate metabolism impairment in chronic kidney disease. *Blood Purif* 27: 338–344.
- Nabeshima Y (2008) The discovery of alpha-Klotho and FGF23 unveiled new insight into calcium and phosphate homeostasis. *Cell Mol Life Sci* 65: 3218–3230.
- Saito H, Kusano K, Kinoshita M, Ito H, Hirata M, et al. (2003) Human fibroblast growth factor-23 mutants suppress Na<sup>+</sup>-dependent phosphate co-transport activity and 1 alpha,25-dihydroxyvitamin D-3 production. *J Biol Chem* 278: 2206–2211.
- Shimada T, Hasegawa H, Yamazaki Y, Muto T, Hino R, et al. (2004) FGF-23 is a potent regulator of vitamin D metabolism and phosphate homeostasis. *J Bone Miner Res* 19: 429–435.
- Ketteler M, Biggar PH, Liangos O (2013) FGF23 antagonism: the thin line between adaptation and maladaptation in chronic kidney disease. *Nephrol Dial Transplant* 28: 821–825.
- Danese MD, Kim J, Doan QV, Dylan M, Griffiths R, et al. (2006) PTH and the risks for hip, vertebral, and pelvic fractures among patients on dialysis. *Am J Kidney Dis* 47: 149–156.
- Alem AM, Sherrard DJ, Gillen DL, Weiss NS, Beresford SA, et al. (2000) Increased risk of hip fracture among patients with end-stage renal disease. *Kidney Int* 58: 396–399.
- Coco M, Rush H (2000) Increased incidence of hip fractures in dialysis patients with low serum parathyroid hormone. *Am J Kidney Dis* 36: 1115–1121.
- Stehman-Breen CO, Sherrard DJ, Alem AM, Gillen DL, Heckbert SR, et al. (2000) Risk factors for hip fracture among patients with end-stage renal disease. *Kidney Int* 58: 2200–2205.
- Parfitt AM (1998) A structural approach to renal bone disease. *J Bone Miner Res* 13: 1213–1220.
- Iwasaki Y, Kazama JJ, Yamato H, Shimoda H, Fukagawa M (2013) Accumulated uremic toxins attenuate bone mechanical properties in rats with chronic kidney disease. *Bone* 57: 477–483.
- Bach-Gansmo FL, Irvine SC, Bruel A, Thomsen JS, Birkedal H (2013) Calcified Cartilage Islands in Rat Cortical Bone. *Calcif Tissue Int* 92: 330–338.
- Shipov A, Zaslansky P, Riesemeier H, Segev G, Atkins A, et al. (2013) Unremodeled endochondral bone is a major architectural component of the cortical bone of the rat (*Rattus norvegicus*). *J Struct Biol* 183: 132–140.
- Polzin DJ (2010) Chronic kidney disease. In: Ettinger SJ, Feldman EC, editors. *Textbook of Veterinary Internal Medicine*. 7th ed. St. Louis: Saunders. pp. 1990–2020.



19. Hillier ML, Bell LS (2007) Differentiating human bone from animal bone: A review of histological methods. *J Forensic Sci* 52: 249–263.
20. Segev G, Palm C, LeRoy B, Cowgill LD, Westropp JL (2013) Evaluation of neutrophil gelatinase-associated lipocalin as a marker of kidney injury in dogs. *J Vet Intern Med* 27: 1362–1367.
21. Zebaze RM, Ghasem-Zadeh A, Bohte A, Iuliano-Burns S, Mirams M, et al. (2010) Intracortical remodelling and porosity in the distal radius and post-mortem femurs of women: a cross-sectional study. *Lancet* 375: 1729–1736.
22. Bousson V, Meunier A, Bergot C, Vicaut E, Rocha MA, et al. (2001) Distribution of intracortical porosity in human midfemoral cortex by age and gender. *J Bone Miner Res* 16: 1308–1317.
23. Montanari S, Brusatte SL, De Wolf W, Norell MA (2011) Variation of osteocyte lacunae size within the tetrapod skeleton: implications for palaeogenomics. *Biol Lett* 7: 751–754.
24. Urbanova P, Novotny V (2005) Distinguishing between human and non-human bones: Histometric method for forensic anthropology. *Anthropologie* 43: 77–85.
25. Currey JD, Shahar R (2013) Cavities in the compact bone in tetrapods and fish and their effect on mechanical properties. *J Struct Biol* 183: 107–122.
26. Kuchler U, Pflingster G, Busenlechner D, Dobsak T, Reich K, et al. (2013) Osteocyte lacunar density and area in newly formed bone of the augmented sinus. *Clin Oral Implants Res* 24: 285–289.
27. Tazawa K, Hoshi K, Kawamoto S, Tanaka M, Ejiri S, et al. (2004) Osteocytic osteolysis observed in rats to which parathyroid hormone was continuously administered. *J Bone Miner Metab* 22: 524–529.
28. Cohen L, Dean M, Shipov A, Atkins A, Monsonego-Ornan E, et al. (2012) Comparison of structural, architectural and mechanical aspects of cellular and acellular bone in two teleost fish. *J Exp Biol* 215: 1983–1993.
29. Sharif A, Barak MM, Shahar R (2008) Whole bone mechanics and mechanical testing. *Vet J* 177: 8–17.
30. Spatz HC, O'Leary EJ, Vincent JF (1996) Young's moduli and shear moduli in cortical bone. *Proc Biol Sci* 263: 287–294.
31. Draper ER, Goodship AE (2003) A novel technique for four-point bending of small bone samples with semi-automatic analysis. *J Biomech* 36: 1497–1502.
32. Turner CH, Burr DB (1993) Basic biomechanical measurements of bone: a tutorial. *Bone* 14: 595–608.
33. Miller MA, Chin J, Miller SC, Fox J (1998) Disparate effects of mild, moderate, and severe secondary hyperparathyroidism on cancellous and cortical bone in rats with chronic renal insufficiency. *Bone* 23: 257–266.
34. Cao HH, Nazarian A, Ackerman JL, Snyder BD, Rosenberg AE, et al. (2010) Quantitative P-31 NMR spectroscopy and H-1 MRI measurements of bone mineral and matrix density differentiate metabolic bone diseases in rat models. *Bone* 46: 1582–1590.
35. Iwasaki Y, Kazama JJ, Yamato H, Fukagawa M (2011) Changes in chemical composition of cortical bone associated with bone fragility in rat model with chronic kidney disease. *Bone* 48: 1260–1267.
36. Jokihaara J, Jarvinen TLN, Jolma P, Koobi P, Kalliovalkama J, et al. (2006) Renal insufficiency-induced bone loss is associated with an increase in bone size and preservation of strength in rat proximal femur. *Bone* 39: 353–360.
37. Nickolas TL, Stein EM, Dworakowski E, Nishiyama KK, Komandah-Kossef M, et al. (2013) Rapid cortical bone loss in patients with chronic kidney disease. *J Bone Miner Res* 28: 1811–1820.
38. Barou O, Valentin D, Vico L, Tirode C, Barbier A, et al. (2002) High-resolution three-dimensional micro-computed tomography detects bone loss and changes in trabecular architecture early: comparison with DEXA and bone histomorphometry in a rat model of disuse osteoporosis. *Invest Radiol* 37: 40–46.
39. Nickolas TL, Leonard MB, Shane E (2008) Chronic kidney disease and bone fracture: a growing concern. *Kidney Int* 74: 721–731.
40. Yencheck RH, Ix JH, Shlipak MG, Bauer DC, Rianon NJ, et al. (2012) Bone mineral density and fracture risk in older individuals with CKD. *Clin J Am Soc Nephrol* 7: 1130–1136.
41. Wasnich RD, Ross PD, Davis JW, Vogel JM (1989) A Comparison of Single and Multi-Site Bmc Measurements for Assessment of Spine Fracture Probability. *J Nucl Med* 30: 1166–1171.
42. Balon BP, Hojs R, Zavrtnik A, Kos M (2002) Bone mineral density in patients beginning hemodialysis treatment. *Am J Nephrol* 22: 14–17.
43. Rix M, Andreassen H, Eskildsen P, Langdahl B, Olgaard K (1999) Bone mineral density and biochemical markers of bone turnover in patients with predialysis chronic renal failure. *Kidney Int* 56: 1084–1093.
44. Leonard MB (2009) A Structural Approach to Skeletal Fragility in Chronic Kidney Disease. *Semin Nephrol* 29: 133–143.
45. van Lenthe GH, Voide R, Boyd SK, Muller R (2008) Tissue modulus calculated from beam theory is biased by bone size and geometry: implications for the use of three-point bending tests to determine bone tissue modulus. *Bone* 43: 717–723.
46. Torcasio A, Van Oosterwyck H, van Lenthe GH (2008) The systematic errors in tissue modulus of murine bones when estimated from three-point bending. *J Biomech* 41: S14.
47. Nickolas TL, Stein E, Cohen A, Thomas V, Staron RB, et al. (2010) Bone mass and microarchitecture in CKD patients with fracture. *J Am Soc Nephrol* 21: 1371–1380.